Polym. Korea, Vol. 45, No. 1, pp. 134-142 (2021)
https://doi.org/10.7317/pk.2021.45.1.134

ISSN 0379-153X(Print)
ISSN 2234-8077(Online)

Fluorene을 기본골격으로 한 공액형 고분자 전해질을 Interlayer로 적용한 고분자태양전지의 광전효과

이준호[#] · 사브리나 아우파 살마[#] · 정미진 · 김주현[†]

부경대학교 고분자공학과

(2020년 9월 10일 접수, 2020년 9월 28일 수정, 2020년 10월 9일 채택)

Investigation of Photovoltaic Properties of Polymer Solar Cells with Fluorene-based Polyelectrolytes as the Interlayer

Junho Lee[#], Sabrina Aufar Salma[#], Mijin Jeong, and Joo Hyun Kim[†]

Department of Polymer Engineering, Pukyong National University, 45 Yongso-ro, Nam-gu, Busan 48513, Korea

(Received September 10, 2020; Revised September 28, 2020; Accepted October 9, 2020)

초록: 고분자의 주사슬 구조가 광전 특성에 어떠한 영향을 미치는지에 관하여 조사하기 위해 고분자 전해질, 6,6'-(2-phenyl-9H-fluorene-9,9-diyl)bis(*N*,*N*,*N*-trimethylhexan-1-aminium) bromide(**PFB-Br**), 6,6'-(2-(thiophen-2-yl)-9H-fluorene-9,9-diyl)bis(*N*,*N*,*N*-trimethylhexan-1-aminium) bromide(**PFT-Br**), 6,6'-(2-([2,2'-bithiophen]-5-yl)-9H-fluorene-9,9-diyl)bis(*N*,*N*,*N*-trimethylhexan-1-aminium) bromide(**PF2T-Br**)을 합성하여 유기 태양광 소자의 중간층으로 도입하였다. 이온성 곁사슬은 스핀 코팅 과정 도중에 ZnO와 상호 작용으로 인해 ZnO 표면으로 자발적으로 배향되며, 주사슬은 반대 방향으로 재배열된다. 고분자 전해질의 재배열로 인해 소자에서 일정한 배향을 가지는 영구 쌍극자가 형성됨으로써, 추가적인 내부 자기장이 형성된다. 주사슬에 도입된 벤젠에 비해 높은 전자 밀도를 가지는 thiophene과 bithiophene에 의해 서로 다른 전자친화도를 가지게 되어 PFT-Br, PF2T-Br의 전자 전달이 방해되고 PFB-Br에 비하여 더 낮은 전력 변환 효율을 나타냄을 확인하였다.

Abstract: A series of conjugated polyelectrolytes (CPEs) based on fluorene named 6,6'-(2-phenyl-9H-fluorene-9,9-diyl)bis(*N*,*N*,*N*-trimethylhexan-1-aminium) bromide (**PFB-Br**), 6,6'-(2-(thiophene-2-yl)-9H-fluorene-9,9-diyl)bis(*N*,*N*,*N*-trimethylhexan-1-aminium) bromide (**PFT-Br**), and 6,6'-(2-([2,2'-bithiophen]-5-yl)-9H-fluorene-9,9-diyl)bis(*N*,*N*,*N*-trimethylhexan-1-aminium) bromide (**PF2T-Br**) were synthesized and applied as the interlayer to investigate how the backbone structure influence the photovoltaic properties. The ionic functionality of CPE accumulates on the ZnO surface, owing to the existing interactions between the ionic groups and the ZnO. The CPE backbone is shifted toward the ZnO surface. Thus, there is a formation of interface dipole via the re-organization of the ionic side chains and hydrophobic backbone. However, incorporation of the electron-rich moiety, thiophene, or bithiophene, in the polymer backbone interfere with the electron transport at the cathode interface. As a result, the power conversion efficiency (PCE) of polymer with thiophene and bithiophene backbone structure was decreased compare with **PFB-Br**, which has electron-affinity property than **PFT-Br**, and **PF2T-Br**.

Keywords: polymer solar cell, fluorene-based polyelectrolyte, thiophene, cathode interlayer.

Introduction

Polymer solar cells (PSCs) have much appeal due to their advantages, such as flexibility, lightweight, wide-area applications, and cost-effectiveness to manufacture. The record power conversion efficiency (PCE) have reached over 16%[1-6] because of the outstanding progress of materials synthesis and device fabrication. The inverted PSCs (iPSCs) device architecture is one of the practical approaches to enhance the stability of the devices, simplify, and lowering the manufacturing cost.[7,8] In the inverted PSCs, inorganic metal oxide (e.g., TiOx or zinc oxide) have been used as interfacial layers due to their capability for improving electron collection and their solution processability.[9-12] Moreover, the light intensity in an active

[#]These authors equally contributed to this work.
[†]To whom correspondence should be addressed.
jkim@pknu.ac.kr, ORCID 0000-0002-1507-1640

layer could be redistributed by the inorganic metal oxide, thus improve the light-harvesting.[13] The pivotal point to iPSCs performance is the transporting material (interlayer) for electron transport or hole-blocking layer. The interlayer material should overcome the formation of Schottky contact between the cathode with LUMO level of the active layer. The HOMO level of the interlayer should be lower than the HOMO of donor material, and the LUMO of the interlayer must be similar to an acceptor material. The interfacial layer also should not be dissolved in the solvent that is used for active layer processing.[14,15] Thus, many studies try to explore a variety of interlayer material to modify the energy level and improve its solubility in MeOH leading to orthogonal solubility with the active layer.

In the conventional PSCs, poly(3,4-ethylenedioxy thiophene): poly(styrene sulfonate) (PEDOT: PSS) is used as an interface layer to modify the ITO electrode.[16,17] However, the use of PEDOT: PSS in the conventional PSCs affects rapid degradation, a short lifetime, and its acidic and hydrophobic properties. Also, the low work function of the metal anode is sensitive to oxygen and moisture.[17-19] Whereas the iPSCs allow the use of less air-sensitive high work function metal, leading to better device stability, compare to conventional PSCs. Most of the devices apply ZnO as a passivation layer owing to ZnO show high performance compare with another interlayer. ZnO is the right choice for n-type semiconductors due to the low cost, high stability, facile synthesis, passivating surface defect, and favorable optical/electronic properties.[11,20-22] The work function of ZnO is 4.40 eV that adequate energy level to lower the work function of the metal electrode or ITO and compatible with the LUMO level of various fullerene active material. The modification of ZnO material is still needed due to the characteristic of binary ZnO and defects within ZnO. The interface between the organic bulk heterojunction (BHJ) active layer and inorganic metal oxide ZnO has an unfavorable contact surface, thus limiting the transport efficiency and resulting in poor short-circuit current density (J_{sc}) and low fill factor (FF).[23-25] Modification of interfacial engineering in the ZnO layer is one of the strategies to enhance the PCEs. The surficial defect on the ZnO layer conquered by applying organic interlayer materials such as self-assembled monolayer, ionic liquid materials, conjugated polymer electrolyte, and fullerene derivatives have been utilized to modify the ZnO layer.[25-31] Recently, conjugated polyelectrolyte (CPE) arise as a good design for the interlayer modifier due to its delocalized π-π conjugated backbone with the ionic group. The devices with CPEs as the interlayer facilitated the electron transport and collection by the formation of interface dipole at the ZnO interface, which improves the device performance. The dipole moment of the CPE is determined by the spontaneous orientation of the ionic chain, which reduces the work function of metal oxide cathode.[23,32-39]

In this work, we fabricated iPSCs by using ZnO film with CPEs as an interlayer. Interestingly, CPEs on the ZnO surface re-modulate the interfacial interaction, reducing the energy offset and increasing the charge collection capability.[37,40-42] The CPEs in this work are composed of the various backbone structure by inserting different moieties, including polyfluorene with phenyl (**PFB**), polyfluorene with thiophene (**PFT**), and polyfluorene with bithiophene (**PF2T**). The CPEs were designed and synthesized to study the effect of the backbone structure that could influence the performance of the device. To avoiding intermixing (*orthogonal-solubility*) with the active layer, the polymers have been quaternarized with trimethylamine. Thus, the CPEs can be processed from the alcoholic solvent. The structure of CPEs have the hydrophobic characteristics in the main chains, and the side chain has hydrophilic characteristics due to the ionic part at the end of the alkyl chain. Thus, quaternarized polyfluorene with trimethylamine, which alters solubility, can be an alternative for increasing device performance.[43] Ionic functionalities in the CPEs are accrued on the ZnO surface owing to attractive interaction between the ionic salts and the hydrophilic ZnO. This indicates that the re-organization of CPEs occurs during the formation of CPE film.[44] Also, the CPE backbone is directed away from the ZnO surface. Consequently, there are formation of interface dipole due to a redistribution of the internal electric field.[45,46] As mentioned above, **PFB-Br**, **PFT-Br**, and **PF2T-Br** have different electronic properties of backbone, **PFT-Br**, and **PF2T-Br** have more electron-rich backbone than **PFB-Br**. Detailed investigations are performed to reveal the effect of various CPE backbone in iPSCs. As a result, the devices based on ZnO/CPE improve the power conversion efficiency compared to the device based on ZnO only. The PCE of the devices with CPE **PFB-Br**, **PFT-Br**, and **PF2T-Br** was 7.98% (J_{sc} = 14.6 mA/cm^2, V_{oc} = 0.76 V, FF = 67.0%), 7.95% (J_{sc} = 15.9 mA/cm^2, V_{oc} = 0.73 V, FF = 67.9%), and 7.95% (J_{sc} = 15.3 mA/cm^2, V_{oc} = 0.72 V, FF = 66.1%). The device based on ZnO has a typical open-circuit voltage (V_{oc}) of 0.76 V, a short-circuit current density (J_{sc}) of 14.6 mA/cm^2, and fill factor (FF) of 67.0% and PCE 7.41%. The main contribution for enhancing the PCE was the improvement of J_{sc}.

Results and Discussion

A series of CPEs with a different backbone were synthesized following modified polymerization procedures (Scheme S1),[37,47,48] details about syntheses and characterization are given in Supporting Information. The polymerization reaction was also introduced according to the previous work.[49] The chemical structure of quaternarized CPEs was shown in Figure 1, along with the inverted device structure. The optical properties of the three types of fluorene CPE are shown in Figure S1. UV-Vis absorption spectra were measured in solution and film. The absorption onset and absorption maximum of **PFB-Br** film appeared at 418 nm and 375 nm, respectively. In the case of **PFT-Br** film, the onset and absorption maximum appeared at 497 nm and 444 nm, respectively. The absorption maximum of **PF2T-Br** was shifted to a longer wavelength than **PFB-Br** and **PFT-Br** due to stronger electron-donating properties of thiophene and bithiophene group. The absorption maximum of **PF2T-Br** appeared at 523 nm and the onset at 462 nm. The optical bandgap for **PFB-Br**, **PFT-Br**, and **PF2T-Br** were 2.97, 2.49, and 2.37 eV, respectively. **PFB-Br** exhibits a bigger optical bandgap compare to that of PFT-Br and **PF2T-Br** because thiophene and bithiophene group are more electron-rich than phenyl group.[50] The cyclic voltammograms (Figure S2) of the CPEs were measured for estimating the energy levels. The HOMO energy levels of **PFB-Br**, **PFT-Br**, and **PF2T-Br** were -5.55, -5.36, and -5.22 eV, respectively. The LUMO levels figured out from the HOMO and the optical band gap were -2.58, -2.87, and -2.85 eV, respectively. Noticeably, **PF2T-Br** exhibits the highest the HOMO level and the lowest LUMO level due to the electron-rich bithiophene unit in the backbone.

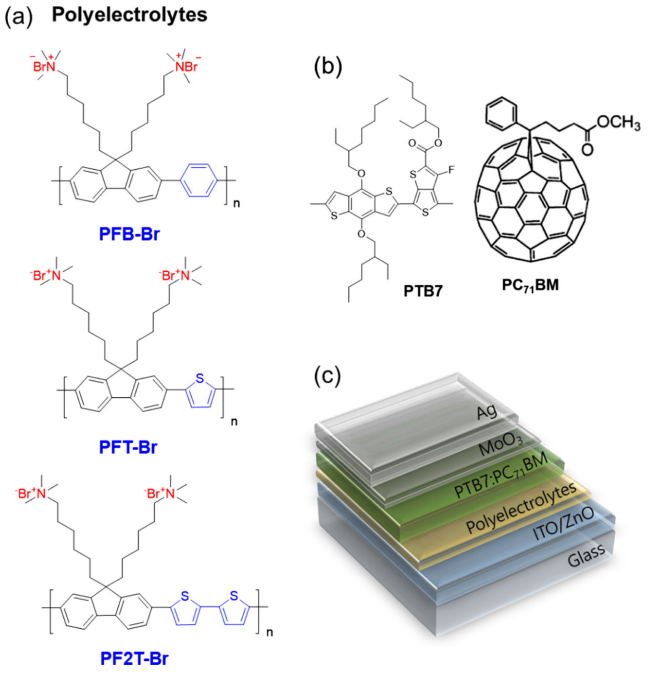

Figure 1. Chemical structure of (a) conjugated polyelectrolytes; (b) PTB7 and $PC_{71}BM$; (c) device architecture of iPSC in this research.

PFB-Br, **PFT-Br**, and **PF2T-Br** were applied as the interlayer in inverted bulk heterojunction (BHJ) iPSCs with device configuration ITO/ZnO/CPE/PTB7:$PC_{71}BM$/MoO_3/Ag. Detailed fabrication procedures of PSCs are described in Supporting Information, and the performances of the devices with CPEs as the interlayer are summarized in Table 1. We investigated the effect of different backbone functionality on the photovoltaic properties. Figure 2 shows the current density (J) *vs.* voltage curves (V) of PSCs with the optimum condition under AM 1.5G solar illumination at 100 $mWcm^{-2}$ and under dark conditions. The performance of the devices with CPEs as interlayer exhibited significant enhancement by comparing those of the device with pristine. The optimum thickness of the interlayer showing the best PCE was determined to be 3 nm. In the device based on pristine ZnO, a typical open-circuit voltage (V_{oc}) of 0.76 V, a short-circuit current density (J_{sc}) of 14.6 $mAcm^{-2}$, and a fill factor (FF) of 67.0% and PCE 7.41%. The PCE of the devices with CPE **PFB-Br**, **PFT-Br**, and **PF2T-Br** was 7.98% (J_{sc} = 14.6 mA/cm^2, V_{oc} = 0.76 V, FF = 67.0%), 7.95% (J_{sc} = 15.9 mA/cm^2, V_{oc} = 0.73 V, FF = 67.9%), and 7.95% (J_{sc} = 15.3 mA/cm^2, V_{oc} = 0.72 V, FF = 66.1%), respectively. These results showed that the stacked interlayer of ZnO/CPE gives excellent interface properties. The main contribution for enhancing the performance of the devices with interlayer was the improvement of J_{sc}. Regardless of the high HOMO and LUMO energy level of CPEs, CPEs reduces a Schottky barrier at the cathode.[45,51] The solar cell incorporating interlayer of **PFB-Br**, **PFT-Br**, and **PF2T-Br**, exhibited almost identical V_{oc}, and FF except J_{sc}. The performances of the device based on **PFT-Br** showed slightly lower than those of the device based on **PFB-Br**. However, the PCE of the PSC based on **PF2T-Br** exhibited the lowest PCE among the devices.

We performed Kelvin probe microscopy (KPM) measurements to investigate the effect of interlayer on the work function of ZnO.[21,52-57] The charge collection interrupt in the devices due to a larger Schottky barrier. Therefore, the formation of Ohmic contact is one of the critical factors in achieving a high J_{sc}. As shown in Figure 3, the work function of ZnO with **PFB-Br**, **PFT-Br**, and **PF2T-Br** were -4.00, -4.01, and

Table 1. Photovoltaic Performances of PSCs with the Best PCE. The Averages of 20 Devices are Shown in Parentheses

Interlayer	Thickness (nm)	J_{sc} (mA/cm^2)	$J_{sc,cal}$[a] (mA/cm^2)	V_{oc} (V)	FF (%)	PCE (%)	R_s[b] (Ω cm^2)
None	-	14.6 (14.5)	14.9	0.76 (0.75)	67.0 (66.8)	7.41 (7.31)	2.91
PFB-Br	5 nm	15.0 (14.9)	-	0.75 (0.75)	66.4 (66.2)	7.48 (7.43)	-
	4 nm	15.6 (15.5)	-	0.74 (0.74)	66.8 (67.0)	7.72 (7.69)	-
	3 nm	15.9 (15.8)	15.7	0.73 (0.73)	68.6 (68.3)	7.98 (7.89)	1.93
PFT-Br	5 nm	15.6 (15.2)	-	0.75 (0.75)	68.1 (67.3)	7.96 (7.66)	-
	3 nm	16.0 (15.8)	16.1	0.73 (0.73)	67.9 (67.9)	7.95 (7.84)	2.13
PF2T-Br	5 nm	14.4 (14.3)	-	0.75 (0.75)	65.4 (63.6)	7.04 (6.85)	-
	3 nm	15.3 (15.2)	15.5	0.72 (0.72)	66.1 (66.0)	7.28 (7.20)	2.53

[a]Calculated from IPCE curves. [b]Series resistance data are calculated from the device showing the best PCE.

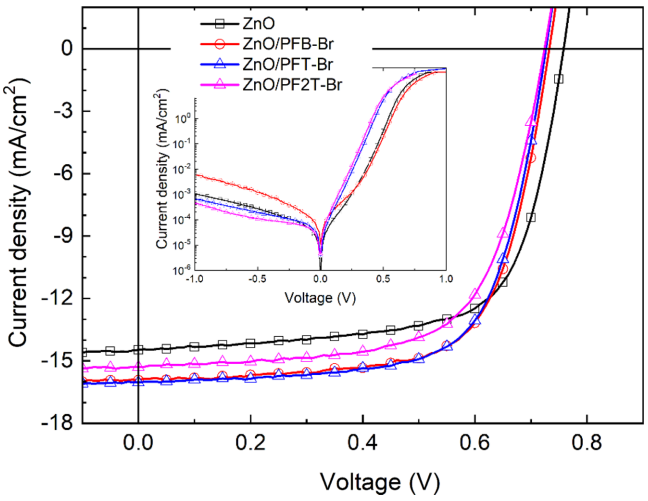

Figure 2. Current density–voltage curves of PSCs under illumination (inset: under dark conditions).

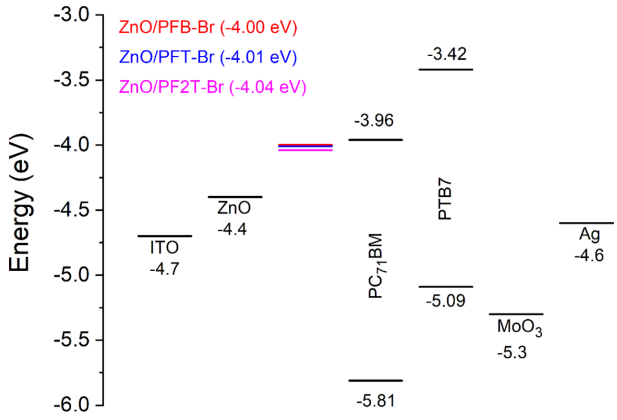

Figure 3. Energy level diagram of materials in this research.

-4.04 eV, respectively, while the work function of ZnO was -4.4 eV. The change of the ZnO work function after introducing CPE indicates the reduction of Schottky barrier height and improvement in J_{sc}. Herein, it was founded that the J_{sc} improvement indicates the formation of favorable interface dipole. The work function of CPE was slightly different from **PFB-Br**, **PFT-Br**, and **PF2T-Br**. However, the change in the work function of ZnO not dependent upon changing the backbone structure of CPE. Calculated J_{sc} data from the IPCE curves (Figure S3) were coherent with the change J_{sc} data obtained from the devices under 1.0 sun condition.

The R_s data were calculated from the inverse slope near the high current region in the dark J-V curves. The R_s value of the ZnO, **PFB-Br**, **PFT-Br**, and **PF2T-Br** were 2.91, 1.93, 2.13, and 2.53 W cm^2, respectively. The decrease in R_s is a vital point in achieving a high FF.[58-61] As summarized in Table 1, the devices with CPE display lower the R_s than pristine, and **PFB-Br** based device displays the lowest R_s among **PFT-Br** and **PF2T-Br** based devices. It's related with the energy barrier at the interface resulted in higher PCE.[45,56] The R_s of **PFT-Br** and **PF2T-Br** are higher than **PFB-Br**. The trade-off between the

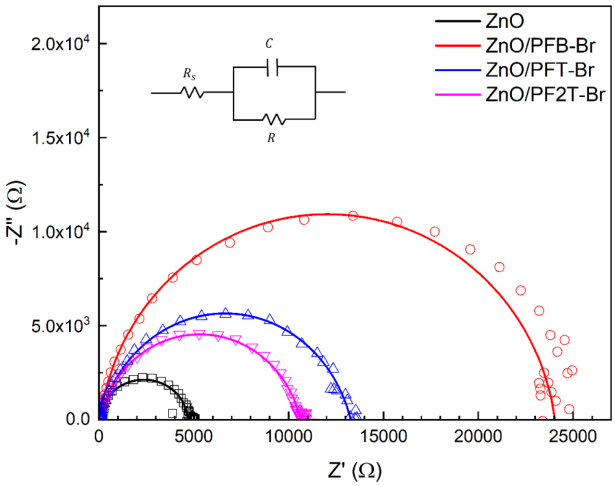

Figure 4. EIS spectra of the PSCs (inset represents the equivalent circuit for analysis, R_s: Ohmic resistance related to the electrodes and the bulk, R: resistance related with the interface charge transport, C: capacitance)

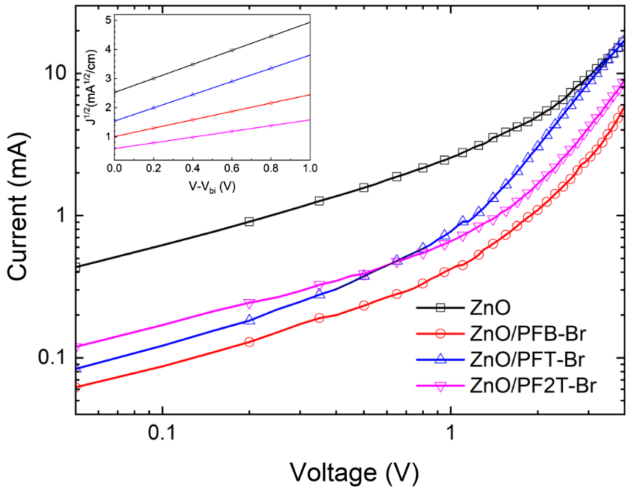

Figure 5. Current density *vs.* voltage curves of the electron-only devices (inset: with a fitted line, V: applied voltage, V_{bi}: built-in voltage).

benefit of a favorable interfacial dipole and the mismatch of the backbone structure reduces the efficiency of inserting thiophene and bithiophene. **PFB-Br**, which has high electron-affinity owing to benzene moiety, shows facile electron collection. On the other hand, **PFT-Br** and **PF2T-Br** show inhibited electron collection induced from an abundant electron density of backbone structure leads to lower PCE compare with **PFB-Br.**

The electrical impedance spectroscopy (EIS) under the dark condition of the devices was performed to investigate the carrier transport and recombination. The EIS measurement showed the Nyquist plots of the PSCs at the V_{oc} condition. The EIS spectra were linearly fitted to calculate the recombination resistance (R_{rec}). The EIS spectra are composed of two depressed semi-circles. In the plot (Figure 4), a high-frequency region corresponds to the response of the photoactive layer, while the lower frequency region corresponds to the response interlayer electrode.[62,63] The semi-circle size of EIS relates to the magnitude of R_{rec} and the amount of the charge recombination in PSCs.[63-65] The R_{rec} of **PFB-Br**, **PFT-Br,** and **PF2T-Br** based devices were 23.87, 12.47, and 10.65 kW, respectively, and 4.75 kW for the device based on pristine ZnO. The device based on ZnO with **PFB-Br** showed the biggest R_{rec}, indicating the minimum recombination at the interface among the devices. The change of R_{rec} coherent with those of the FF of PSCs.

To further investigate the electron injection properties of the iPSCs with different CPEs, we fabricate a device based on electron-only with a structure of ITO/ZnO (25 nm)/CPE/$PC_{71}BM$/Al (100 nm). The electron mobility was estimated using the Mott–Gurney equation (Figure 5). The electron mobility of the electron-only devices with ZnO/**PFB-Br**, **PFT-Br**, **PF2T-Br** was 3.97×10^{-4}, 3.27×10^{-4}, 2.87×10^{-4} $cm^2V^{-1}s^{-1}$, respectively. CPEs shows higher electron mobility than the pristine ZnO (2.1×10^{-4} $cm^2V^{-1}s^{-1}$). The J_{sc} data of the devices with CPEs were improved compared to pristine ZnO. Consequently, electron mobility through the changing of recombination resistance is derived from the CPE backbone orientation. During the spin-coating of CPEs, the ionic groups are moved toward the ZnO layer. In contrast, the hydrophobic part of the polyelectrolyte is shifted toward the surface of the active layer.

The V_{oc} and J_{sc} of the devices vs. illumination intensity was plotted for investigating the charge recombination kinetics. The V_{oc} *vs.* light intensity is briefly defined as $V_{oc} \propto skT/q \ln(I)$. The J_{sc} *vs.* light intensity is defined as $J_{sc} \propto I^{\alpha}$. Where I is the illumination intensity, k, T, and q are the Boltzmann constant, the temperature in Kelvin, and electron charge, respectively. When α values are nearest or equal to 1, the bimolecular recombination is dominated in the entire devices under short circuit conditions. In Figure 6, the value of α based on ZnO/**PFB-Br**, **PFT-Br**, **PF2T-Br** was 0.99, 0.98, and 0.97, respectively.

In contrast, the α value of the ZnO monolayer was 0.968. Noticeably, the α value indicated that the modified layer slightly near to bimolecular recombination. When s value reaches 2, the devices exhibit dominant trap-assisted recombination. However, if the device exhibits the band-to-band recombination, then the n value is near unity.[66] The s values of

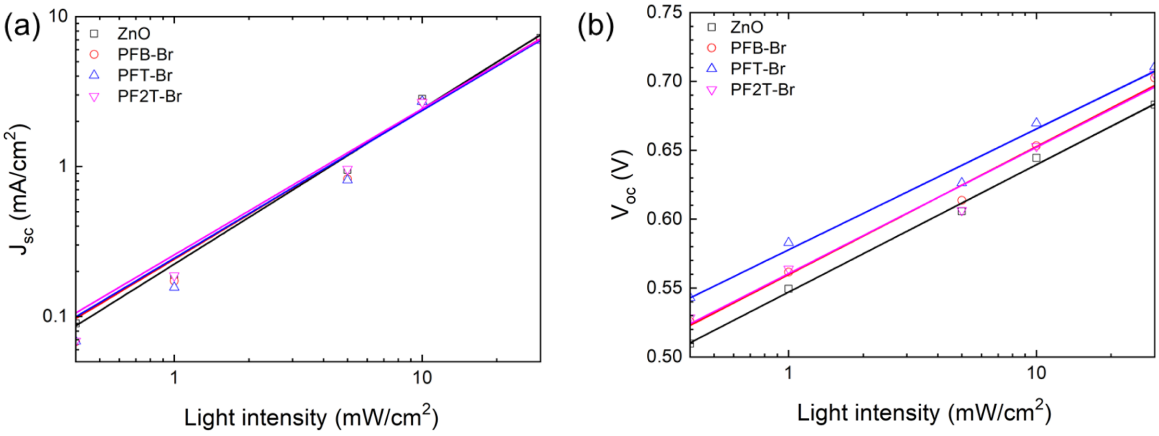

Figure 6. (a) J_{sc}; (b) V_{oc} *vs*. illumination intensity.

the devices with ZnO, ZnO/**PFB-Br**, ZnO/**PFT-Br**, and ZnO/**PF2T-Br**, were 1.56, 1.57, 1.48, and 1.55, respectively. Most of the device parameters related to the charge extraction and recombination of the devices. Those are improved by introducing the conjugated polyelectrolyte interlayer in ZnO. Besides, the change in the α and s values of the devices agree well with the PCE trend of PSCs.[67]

Conclusions

The inverted PSCs with a blend of PTB7:$PC_{71}BM$ were fabricated to investigate the effect of CPEs on the devices. The CPE based on fluorene named **PFB-Br**, **PFT-Br**, and **PF2T-Br**, which have different backbone structures influence the electronic and photovoltaic properties. The efficiency of the device with CPEs as interlayer is higher than the device without CPEs, indicating the reduction of a Schottky barrier. The ionic pendant and organic backbone structure spontaneously reorient to ZnO and active layer during the fabrication process, respectively. Although CPEs has the same ion pendant groups, the PCE of the PSCs with **PFB-Br** is higher than those of the device with **PF2T-Br**. Whereas, **PFB-Br** has better electron-affinity owing to benzene moiety, shows facile electron collection. **PF2T-Br** show inhibited electron collection induced from an abundant electron density of backbone structure leads to lower device efficiency compare with **PFB-Br.**

Acknowledgment(s): This work was supported by the Korea Institute of Energy Technology Evaluation and Planning (KETEP) and the Ministry of Trade, Industry & Energy (MOTIE) of the Republic of Korea (No. 20194010201840) and was supported by the BB21+ Project in 2019.

Supporting Information: Information is available regarding the experimental procedure for the synthesis, measurements, fabrication of polymer solar cells, UV-Vis spectra, CV, and IPCE spectra. The materials are available *via* the Internet at http://journal.polymer-korea.or.kr.

References

1. Mishra, A.; Bäuerle, P. Small Molecule Organic Semiconductors on the Move: Promises for Future Solar Energy Technology. *Angew. Chemie - Int. Ed.* **2012**, 51, 2020-2067.
2. Li, Y.; Zheng, N.; Yu, L.; Wen, S.; Gao, C.; Sun, M.; Yang, R. A Simple Phenyl Group Introduced at the Tail of Alkyl Side Chains of Small Molecular Acceptors: New Strategy to Balance the Crystallinity of Acceptors and Miscibility of Bulk Heterojunction Enabling Highly Efficient Organic Solar Cells. *Adv. Mater.* **2019**, 31, 1807832.
3. Zhang, H.; Yao, H.; Hou, J.; Zhu, J.; Zhang, J.; Li, W.; Yu, R.; Gao, B.; Zhang, S.; Hou, J. Over 14% Efficiency in Organic Solar Cells Enabled by Chlorinated Nonfullerene Small-Molecule Acceptors. *Adv. Mater.* **2018**, 30, 1800613.
4. Meng, L.; Zhang, Y.; Wan, X.; Li, C.; Zhang, X.; Wang, Y.; Ke, X.; Xiao, Z.; Ding, L.; Xia, R.; Hin-Lap Y.; Cao, Y.; Chen, Y. Organic and Solution-processed Tandem Solar Cells with 17.3% Efficiency. *Science* **2018**, 361, 1094-1098.
5. Han, J.; Wang, X.; Huang, D.; Yang, C.; Yang, R.; Bao, X. Employing Asymmetrical Thieno[3,4-d]pyridazin-1(2H)-one Block Enables Efficient Ternary Polymer Solar Cells with Improved Light-Harvesting and Morphological Properties. *Macromolecules* **2020**, 53, 6619-6629.
6. Hoang, M. H.; Park, G. E.; Phan, D. L.; Ngo, T. T.; Nguyen, T. V.; Park, C. G.; Cho, M. J.; Choi, D. H. Synthesis of Conjugated Wide-Bandgap Copolymers Bearing Ladder-Type Donating Units and Their Application to Non-Fullerene Polymer Solar Cells. *Macromol. Res.* **2018**, 26, 844-850.

7. Maduwu, R. D.; Jin, H. C.; Kim, J. H. Synthesis and Characterization of Benzothiadiazole and Dicyanovinylindandione Based Small-Molecular Conjugated Materials and Their Photovoltaic Properties. *Macromol. Res*. **2019**, 27, 1261-1267.
8. Fijahi, L.; Ameen, S.; Akhtar, S. M.; Abdullah; Kim, E.-B.; Kim, T.-G.; Shin, H.-S. Benzothiadiazole with π-Spacer as Efficient Chromophore for Bulk Heterojunction Organic Solar Cells. *Ind. Eng. Chem*. **2019**, 11, 151-158.
9. Kim, J. Y.; Kim, S. H.; Lee, H.-H.; Lee, K.; Ma, W.; Gong, X.; Heeger, A. J. New Architecture for High-Efficiency Polymer Photovoltaic Cells Using Solution-Based Titanium Oxide as an Optical Spacer. *Adv. Mater*. **2006**, 18, 572-576.
10. Roy, A.; Park, S. H.; Cowan, S.; Tong, M. H.; Cho, S.; Lee, K.; Heeger, A. J. Titanium Suboxide as an Optical Spacer in Polymer Solar Cells. *Appl. Phys. Lett*. **2009**, 95, 013302.
11. Kim, Y. H.; Kim, D. G.; Maduwu, R. D.; Jin, H. C.; Moon, D. K.; Kim, J. H. Organic Electrolytes Doped ZnO Layer as the Electron Transport Layer for Bulk Heterojunction Polymer Solar Cells. *SSol. RRL* **2018**, 2, 1800086.
12. Park, S.; Jang, W.; Wang, D. H. Alignment of Cascaded Band-Gap via PCBM/ZnO Hybrid Interlayers for Efficient Perovskite Photovoltaic Cells. *Macromol. Res*. **2018**, 26, 472-476.
13. Gilot, J.; Barbu, I.; Wienk, M. M.; Janssen, R. A. J. The Use of ZnO as Optical Spacer in Polymer Solar Cells: Theoretical and Experimental Study. *Appl. Phys. Lett*. **2007**, 91, 113520.
14. Sun, Y.; Takacs, C. J.; Cowan, S. R.; Seo, J. H.; Gong, X.; Roy, A.; Heeger, A. J. Efficient, Air-Stable Bulk Heterojunction Polymer Solar Cells Using MoOx as the Anode Interfacial Layer. *Am. Chem. Soc*. **2011**, 23, 2226-2230.
15. Motiei, L.; Yao, Y.; Choudhury, J.; Yan, H.; Marks, T. J.; Boom, M. E. van der; Facchetti, A. Self-Propagating Molecular Assemblies as Interlayers for Efficient Inverted Bulk-Heterojunction Solar Cells. *J. Am. Chem. Soc*. **2010**, 132, 12528-12530.
16. Jang, H.; Kim, M. S.; Jang, W.; Son, H.; Wang, D. H.; Kim, F. S. Highly Conductive PEDOT:PSS Electrode Obtained via Post-treatment with Alcoholic Solvent for ITO-free Organic Solar Cells. *Ind. Eng. Chem*. **2020**, 86, 205-210.
17. Yin, Z.; Wei, J.; Zheng, Q. Interfacial Materials for Organic Solar Cells: Recent Advances and Perspectives. *Adv. Sci*. **2016**, 3, 1500362.
18. Jørgensen, M.; Norrman, K.; Krebs, F. C. Stability/Degradation of Polymer Solar Cells. *Sol. Energy Mater. Sol. Cells* **2008**, 92, 686-714.
19. Yin, Z.; Zheng, Q. Controlled Synthesis and Energy Applications of One-Dimensional Conducting Polymer Nanostructures: An Overview. *Adv. Energy Mater*. **2011**, 2, 179-218.
20. Huang, J.; Yin, Z.; Zheng, Q. Applications of ZnO in Organic and Hybrid Solar Cells. *Energy Environ. Sci.* **2011**, 4, 3861.
21. Kim, D. G.; Kim, Y. H.; Maduwu, R. D.; Jin, H. C.; Moon, D. K.; Kim, J. H. Organic Electrolyte Hybridized ZnO as the Electron Transport Layer for Inverted Polymer Solar Cells. *J. Ind. Eng. Chem*. **2018**, 65, 175.
22. Lu, L.; Zheng, T.; Wu, Q.; Schneider, A. M.; Zhao, D.; Yu, L. Recent Advances in Bulk Heterojunction Polymer Solar Cells. *Chem. Rev.* **2015**, 115, 12666-12731.
23. Subbiah, J.; Mitchell, V. D.; Hui, N. K. C.; Jones, D. J.; Wong, W. W. H. A Green Route to Conjugated Polyelectrolyte Interlayers for High-Performance Solar Cells. *Angew. Chemie - Int. Ed*. **2017**, 6, 8431-8434.
24. Ma, H.; Yip, H.-L.; Huang, F.; Jen, A. K.-Y. Interface Engineering for Organic Electronics. *Adv. Funct. Mater.* **2010**, 20, 1371-1388.
25. Liu, C.; Tan, Y.; Li, C.; Wu, F.; Chen, L.; Chen, Y. Enhanced Power-Conversion Efficiency in Inverted Bulk Heterojunction Solar Cells Using Liquid-Crystal-Conjugated Polyelectrolyte Interlayer. *ACS Appl. Mater. Interfaces* **2015**, 7, 19024-19033.
26. Lee, B. R.; Choi, H.; Park, J. S.; Lee, H. J.; Kim, S. O.; Kim, J. Y.; Song, M. H. Surface Modification of Metal Oxide Using Ionic Liquid Molecules in Hybrid Organic-inorganic Optoelectronic Devices. *J. Mater. Chem.* **2011**, 21, 2051-2053.
27. Bulliard, X.; Ihn, S. G.; Yun, S.; Kim, Y.; Choi, D.; Choi, J. Y.; Kim, M.; Sim, M.; Park, J. H.; Choi, W.; Cho, K. Enhanced Performance in Polymer Solar Cells by Surface Energy Control. *Adv. Funct. Mater*. **2010**, 20, 4381-4387.
28. Cheng, Y.-J.; Hsieh, C.-H.; He, Y.; Hsu, C.-S.; Li, Y. Combination of Indene-C60Bis-Adduct and Cross-Linked Fullerene Interlayer Leading to Highly Efficient Inverted Polymer Solar Cells. *J. Am. Chem. Soc*. **2010**, 132, 17381-17383.
29. Li, P.; Li, X.; Sun, C.; Wang, G.; Li, J.; Jiu, T.; Fang, J. Performance Enhancement of Inverted Polymer Solar Cells with Fullerene Ester Derivant-modified ZnO Film as Cathode Buffer Layer. *Sol. Energy Mater. Sol. Cells* **2014**, 126, 36-41.
30. Ha, Y. E.; Jo, M. Y.; Park, J.; Kang, Y.-C.; Yoo, S. I.; Kim, J. H. Inverted Type Polymer Solar Cells with Self-Assembled Monolayer Treated ZnO. *J. Phys. Chem. C* **2013**, 117, 2646-2652.
31. Do, T. T.; Hong, H. S.; Ha, Y. E.; Yoo, S. I.; Won, Y. S.; Moon, M.-J.; Kim, J. H. Synthesis and Characterization of Conjugated Oligoelectrolytes Based on Fluorene and Carbazole Derivative and Application of Polymer Solar Cell as a Cathode Buffer Layer. *Macromol. Res*. **2015**, 23, 367-376.
32. Hoven, C. V.; Garcia, A.; Bazan, G. C.; Nguyen, T.-Q. Recent Applications of Conjugated Polyelectrolytes in Optoelectronic Devices. *Adv. Mater*. **2008**, 20, 3793-3810.
33. Choi, H.; Mai, C.-K.; Kim, H.-B.; Jeong, J.; Song, S.; Bazan, G. C.; Kim, J. Y.; Heeger, A. J. Conjugated Polyelectrolyte Hole Transport Layer for Inverted-type Perovskite Solar Cells. *Nat. Commun*. **2015**, 6, 1-6.
34. Duan, C.; Zhang, K.; Guan, X.; Zhong, C.; Xie, H.; Huang, F.; Chen, J.; Peng, J.; Cao, Y. Conjugated Zwitterionic Polyelectrolyte-based Interface Modification Materials for High Performance Polymer Optoelectronic Devices. *Chem. Sci*. **2013**, 4, 1298-1307.
35. Liu, Y.; Page, Z. A.; Russell, T. P.; Emrick, T. Finely Tuned Polymer Interlayers Enhance Solar Cell Efficiency. *Angew. Chemie - Int. Ed*. **2015**, 54, 11485-11489.
36. Hu, Z.; Zhang, K.; Huang, F.; Cao, Y. Water/Alcohol Soluble

Conjugated Polymers for the Interface Engineering of Highly Efficient Polymer Light-emitting Diodes and Polymer Solar Cells. *Chem. Commun*. **2015**, 51, 5572-5585.
37. Chang, Y.-M.; Leu, C.-Y. Conjugated Polyelectrolyte and Zinc Oxide Stacked Structure as an Interlayer in Highly Efficient and Stable Organic Photovoltaic Cells. *J. Mater. Chem. A* **2013**, 1, 6446.
38. Xia, R.; Leem, D.-S.; Kirchartz, T.; Spencer, S.; Murphy, C.; He, Z.; Wu, H.; Su, S.; Cao, Y.; Kim, J. S.; C. deMello, J.; D. C. Bradley, D.; Nelson, J. Investigation of a Conjugated Polyelectrolyte Interlayer for Inverted Polymer:Fullerene Solar Cells. J. Nelson, *Adv. Energy Mater*. **2013**, 3, 718-723.
39. Baek, G. W.; Kim, Y.-J.; Jung, K.-H.; Han, Y. S. Enhancement of Solar Cell Performance Through the Formation of a Surface Dipole on Polyacrylonitrile-treated TiO_2 Photoelectrodes. *J. Ind. Eng. Chem*. **2019**, 73, 260-267.
40. Woo, S.; Kim, W. H.; Kim, H.; Yi, Y.; Lyu, H.-K.; Kim, Y. 8.9% Single-Stack Inverted Polymer Solar Cells with Electron-Rich Polymer Nanolayer-Modified Inorganic Electron-Collecting Buffer Layers. *Adv. Energy Mater*. **2014**, 4, 1301692.
41. Wu, N.; Luo, Q.; Bao, Z.; Lin, J.; Li, Y.-Q.; Ma, C.-Q. Zinc oxide: Conjugated Polymer Nanocomposite as Cathode Buffer Layer for Solution Processed Inverted Organic Solar Cells. *Sol. Energy Mater. Sol. Cells* **2015**, 141, 248-259.
42. Guo, Y.; Xia, D.; Liu, B.; Wu, H.; Li, C.; Tang, Z.; Xiao, Chengyi; Li, W. Small Band gap Boron Dipyrromethene-Based Conjugated Polymers for All-Polymer Solar Cells: The Effect of Methyl Units. *Macromolecules* **2019**, 52, 8367-8373.
43. Liu, H.; Hu, L.; Wu, F.; Chen, L.; Chen, Y. Polyfluorene Electrolytes Interfacial Layer for Efficient Polymer Solar Cells: Controllably Interfacial Dipoles by Regulation of Polar Groups. *ACS Appl. Mater. Interfaces* **2016**, 8, 9821-9828.
44. Park, J.; Yang, R.; Hoven, C. V.; Garcia, A.; Fischer, D. A.; Nguyen, T.; Bazan, G. C.; DeLongchamp, D. M. Structural Characterization of Conjugated Polyelectrolyte Electron Transport Layers by NEXAFS Spectroscopy. *Adv. Mater*. **2008**, 20, 2491-2496.
45. Jo, M. Y.; Do, T. T.; Ha, Y. E.; Won, Y. S.; Kim, J. H. Enhanced Efficiency in Polymer Solar Cells by Incorporation of Phenothiazine-based Conjugated Polymer Electrolytes. *Org. Electron*. **2015**, 16, 18-25.
46. Jo, M. Y.; Ha, Y. E.; Won, Y. S.; Yoo, S. I.; Kim, J. H. Effect of Side Chain Arrangement of Conjugated Polyelectrolytes Buffer Layer on the Photovoltaic Properties. *Org. Electron*. **2015**, 25, 85-91.
47. Bini, K.; Xu, X.; Andersson, M. R.; Wang, E. Alcohol-Soluble Conjugated Polymers as Cathode Interlayers for All-Polymer Solar Cells. *ACS Appl. Energy Mater*. **2018**, 1, 2176-2182.
48. Qiu, R.; Song, L.; Zhang, D.; Mo, Y.; Brewer, E.; Huang, X. Characterization of Conjugated Polymer Poly(fluorene-*co*-thiophene) and Its Application as Photosensitizer of TiO_2. *Int. J. Photoenergy* **2008**, 164702.
49. Oh, S.-H.; Na, S.-I.; Nah, Y.-C.; Vak, D.; Kim, S.-S.; Kim, D.-Y. Novel Cationic Water-soluble Polyfluorene Derivatives with Ion-transporting Side Groups for Efficient Electron Injection in PLEDs. *Org. Electron*. **2007**, 8, 773-783.
50. Blondin, P.; Bouchard, J.; Beaupré, S.; Belletête, M.; Durocher, G.; Leclerc, M. Molecular Design and Characterization of Chromic Polyfluorene Derivatives. *Macromolecules* **2000**, 33, 5874-5879.
51. Zhang, Z.-G.; Qi, B.; Jin, Z.; Chi, D.; Qi, Z.; Li, Y.; Wang, J. Perylene Diimides: A Thickness-insensitive Cathode Interlayer For High Performance Polymer Solar Cells. *Energy Environ. Sci*. **2014**, 7, 1966-1973.
52. Jo, M. Y.; Ha, Y. E.; Kim, J. H. Polyviologen Derivatives as An Interfacial Layer in Polymer Solar Cells. *Sol. Energy Mater. Sol. Cells* **2012**, 107, 1-8.
53. Jo, M. Y.; Ha, Y. E.; Kim, J. H. Interfacial Layer Material Derived from Dialkylviologen and Sol-gel Chemistry for Polymer Solar Cells. *Org. Electron*. **2013**, 14, 995-1001.
54. Kim, Y. H.; Sylvianti, N.; Marsya, M. A.; Park, J.; Kang, Y.-C.; Moon, D. K.; Kim, J. H. A Simple Approach to Fabricate an Efficient Inverted Polymer Solar Cell with a Novel Small Molecular Electrolyte as the Cathode Buffer Layer. *Org. Electron*. **2016**, 8, 32992-32997.
55. Lim, G. E.; Ha, Y. E.; Jo, M. Y.; Park, J.; Kang, Y.-C.; Kim, J. H. Nonconjugated Anionic Polyelectrolyte as an Interfacial Layer for the Organic Optoelectronic Devices. *ACS Appl. Mater. Interfaces* **2013**, 5, 6508-6513.
56. Do, T. T.; Hong, H. S.; Ha, Y. E.; Park, C.-Y.; Kim, J. H. Investigation of the Property Change of Polymer Solar Cells by Changing Counter Anions in Polyviologen as a Cathode Buffer Layer. *Macromol. Res*. **2015**, 23, 177-182.
57. Jin, H. C.; Salma, S. A.; Moon, D. K.; Kim, J. H. Effect of Conjugated Polymer Electrolytes with Diverse Acid Derivatives as a Cathode Buffer Layer on Photovoltaic Properties. *J. Mater. Chem. A* **2020**, 8, 4562-4569.
58. Liu, S.; Zhang, G.; Lu, J.; Jia, J.; Li, W.; Huang, F.; Cao, Y. An Alcohol Soluble Amino-functionalized Organoplatinum(II) Complex as the Cathode Interlayer for Highly Efficient Polymer Solar Cells. *J. Mater. Chem. C* **2015**, 3, 4372-4379.
59. Wang, Z.; Li, Z.; Xu, X.; Li, Y.; Li, K.; Peng, Q. Ploymer Solar Cells: Polymer Solar Cells Exceeding 10% Efficiency Enabled via a Facile Star-Shaped Molecular Cathode Interlayer with Variable Counterions. *Adv. Funct. Mater*. **2016**, 26, 4803-4803.
60. Yu, W.; Huang, L.; Yang, D.; Fu, P.; Zhou, L.; Zhang, J.; Li, C. Efficiency Exceeding 10% for Inverted Polymer Solar Cells with a ZnO/Ionic Liquid Combined Cathode Interfacial Layer. *J. Mater. Chem. A* **2015**, 3, 10660-10665.
61. Jeong, M.; Jin, H. C.; Moon, D. K.; Kim, J. H. Simple Approach to Overcome Thickness Tolerance of Interlayer without Sacrificing the Performances of Polymer Solar Cells. *Adv. Mater*. **2019**, 6, 1900797.
62. Liu, X.; Jiao, W.; Lei, M.; Zhou, Y.; Song, B.; Li, Y. Crown-ether Functionalized Fullerene as a Solution-processable Cathode Buffer Layer for High Performance Perovskite and Polymer Solar

Cells. *J. Mater. Chem. A* **2015**, 3, 9278-9284.
63. Jeong, M.; Jin, H. C.; Lee, J. H.; Moon, D. K.; Kim, J. H. Effect of Interface Modification in Polymer Solar Cells: An In-depth Investigation of the Structural Variation of Organic Dye for Interlayer Material. *Dyes Pigm*. **2020**, 173, 107927.
64. Kim, H.; Jeong, H.; An, T. K.; Park, C. E.; Yong, K. Hybrid-Type Quantum-Dot Cosensitized ZnO Nanowire Solar Cell with Enhanced Visible-Light Harvesting. *ACS Appl. Mater. Interfaces* **2012**, 5, 268-275.
65. Wang, H.; Liu, G.; Li, X.; Xiang, P.; Ku, Z.; Rong, Y.; Han, H. Highly Efficient Poly(3-hexylthiophene) Based Monolithic Dye-sensitized Solar Cells with Carbon Counter Electrode. *Energy Environ. Sci*. **2011**, 4, 2025-2029.
66. Yang, F.; Li, J.; Li, C.; Li, W. Improving Electron Transport in a Double-Cable Conjugated Polymer via Parallel Perylenetriimide Design. *Macromolecules* **2019**, 52, 3689-3696.
67. Tyagi, H.; Agarwal, A. K.; Chakraborty, P. R.; Powar, S., Eds., *Advances in Solar Energy Research. Energy, Environment, and Sustainability*; Springer, Singapore, 2019.